BeBeC-2012-11

THREE-DIMENSIONAL ACOUSTIC SOURCE MAPPING

Ennes Sarradj
Chair of Technical Acoustics
Brandenburg University of Technology Cottbus
Siemens-Halske-Ring 14, 03046 Cottbus, Germany

ABSTRACT

When beamforming is applied for acoustic source mapping, the sound pressure contributions of any sound sources are most often mapped to a planar or a surface map. However, some practical applications would benefit from a three-dimensional mapping, where the map consists of a three-dimensional grid. It is shown that the extension of microphone array beamforming techniques to three-dimensional mapping is straightforward in principle, but requires the mandatory use of deconvolution techniques. Feasible deconvolution approaches and their practical implementation are discussed. While the computational cost is considerable higher than for classical two-dimensional mapping, the three-dimensional approach provides a number of advantages and easily delivers correct information on the source level by using an adopted integration technique. Finally, the three-dimensional mapping is demonstrated and the results of practical applications are shown and discussed.

1 INTRODUCTION

Acoustic source mapping based on beamforming techniques is used to study a great variety of different acoustic sources. This includes sources on vehicles, engines, machinery and on other installations. A typical application is to analyse the location and the strength of a source or, more often, of a number of sources simultaneously. Such analysis assumes a certain model for the sources and sound field, e.g. monopole sources in a free sound field. A microphone array is then used to simultaneously collect sound pressure data at different locations. Then, a beamforming technique is used to construct a map from this data.

The map projects an indicator quantity for the source strength (e.g. some sort of sound pressure level) onto a grid, thus producing an image of acoustic source distribution. This acoustic source mapping indicates the spatial regions where sources reside and generally allows to estimate both location and strength of sources. Depending on the array, the wavelength and the signal processing algorithm used, the source mapping may be blurred and may also exhibit ambiguous features. The majority of practical applications of this kind of source mapping reported in the literature use planar or surface grids for the map.

Without a priori knowledge of the source location, this restricts the information about the location of sources to the mapping surface. Real sources exist in three-dimensional space and not necessarily on a surface. However, with such two-dimensional mapping there is no way to tell if a mapped source is not located on the surface. Because the location of a source must be known for the estimation of its strength from far-field measurements, this circumstance renders the estimation of the source strength imprecise if the source is not on the surface. On the other hand, this can only be improved by using a three-dimensional grid for acoustic source mapping.

While the extension of two-dimensional to three-dimensional mapping is straightforward, only few attempts of three-dimensional source mapping were reported (e.g. [2, 4–7]). The computational expenses are generally much greater and the gain in information is limited by a poor spatial resolution along the third axis. That is why in many practical situations the disadvantages of two-dimensional mapping are presently accepted. Here, the problems and specifics of three-dimensional beamforming shall be discussed and some practical experiences shall be presented.

2 THEORY

In general, beamforming can be seen as applying a spatial filter to the distribution of sound sources within a sound field. The filtering process takes the microphone sound pressures p_i representing the sound field as input data. The beamformer filter is then realised in the frequency domain by calculating the weighted sum of the microphone sound pressures (vector $\mathbf{p}$) using complex-valued weight factors. The vector $\mathbf{h}(\mathbf{x}_t)$ of these factors is the steering vector and governs the characteristics of the filter. It depends on an assumed source location $\mathbf{x}_t$ and on the model used for the sources and the sound field. The filter output is:

$$p_F(\mathbf{x}_t) = \mathbf{h}(\mathbf{x}_t)^{\mathrm{H}}\mathbf{p}, \tag{1}$$

with the superscript H denoting the hermitian transpose. If an acoustic source is present at $\mathbf{x}_t$, the output p_F is a representation of its signal. A commonly used paradigm in the design of the filter, i.e. in the choice of $\mathbf{h}(\mathbf{x}_t)$, is that p_F is the contribution of the source at $\mathbf{x}_t$ to the sound pressure at a reference location, often the centre of the microphone array.

The strength, or amplitude of the signal is a statistical quantity that can be estimated either directly from p_F or from the auto power spectrum $B(\mathbf{x}_t) = E\{p_F(\mathbf{x}_t)p_F^*(\mathbf{x}_t)\}$, where $E\{\}$ is the expectation operator. The latter option makes it possible to use the estimated cross spectral matrix of microphone signals $\mathbf{G}$ for the calculation:

$$B(\mathbf{x}_t) = \mathbf{h}^{\mathrm{H}}(\mathbf{x}_t)E\{\mathbf{p}\mathbf{p}^{\mathrm{H}}\}\mathbf{h}(\mathbf{x}_t) = \mathbf{h}^{\mathrm{H}}(\mathbf{x}_t)\mathbf{G}\mathbf{h}(\mathbf{x}_t). \tag{2}$$

For the construction of a map this calculation must be repeated for every grid point, i.e. for different $\mathbf{x}_t$. In this case, $\mathbf{G}$ needs to be calculated only once. Because there is no further assumption about $\mathbf{x}_t$, (2) can be applied in the same way for both two- and three-dimensional grids (and also for one-dimensional grids). However, it turns out that the filter properties are very different in different directions seen from the array (see section 3).

Acoustic source mapping can be seen as an imaging operation where an image $B(\mathbf{x})$ of an actual spatial distribution $A(\mathbf{x})$ (e.g. a 'monopole density') is produced by an imaging system. While a perfect imaging system would produce $B = A$, any real, but linear system, and thus also

the use of beamforming, produces

$$B(\mathbf{x}_t) = P(\mathbf{x}_t, \mathbf{x}_s) * A(\mathbf{x}_s). \tag{3}$$

$*$ is the spatial convolution operation and P is the spatial impulse response of the imaging system, also termed point spread function (PSF). The PSF depends on $\mathbf{h}$ and on the model assumed for the sources and the sound field. It governs the usable spatial resolution and any ambiguities in the image (also known as side lobes in one-dimensional representations of the PSF). To mitigate this imperfections, a number of deconvolution methods can be used to 'remove' the PSF from the result, i.e. to estimate the true or actual distribution A from the image B.

Some deconvolution methods such as DAMAS[3] and some derived methods try to solve (3) as an inverse problem and require the a priori estimation of the complete PSF. In view of a three-dimensional application the latter is most important. If N is the number of grid points, then the (discrete) PSF consists of N^2 values that must be estimated. Even if certain assumptions about the spatial variance of the PSF are applied that reduce the number of values to be estimated, this number increases roughly with N^2. Because a three-dimensional mapping typically requires two orders of magnitude greater N compared to a two-dimensional mapping, the computational cost for the PSF increases by four orders of magnitude. This renders the application of these kind of methods inefficient. Moreover, the effort for the solution of the inverse problem itself increases roughly with N^2.

Other methods such as CLEAN-SC[9] and orthogonal beamforming[8] make use of certain assumptions to estimate the actual PSF from the measured data and the image. In this case the computational cost increases roughly with N. For three-dimensional application this means an increase of typically two orders of magnitude. While this is certainly much more than for two-dimensional mapping, it is still feasible.

3 RESULTS

A first example result that should be discussed here is from the measurement of aerofoil leading edge noise [6] in the aeroacoustic wind tunnel of Brandenburg University of Technology at Cottbus. The aerofoil under test had an SD7003 cross-section (for further details see Fig. 1). The inflow turbulence required for the generation of aerofoil leading edge noise was provided by grids mounted to the nozzle exit of the open jet wind tunnel. Besides the use of different turbulence grids, the distance between the grids and the airfoil leading edge position can be varied, thus providing a larger range of different incident turbulence parameters. These parameters were measured using hot–wire anemometry. Here, the discussion shall be restricted to only one case with a square grid of 12 mm grid width that generates a turbulence intensity of about 10%. Moreover, only the results for a flow speed of 45 m/s are shown.

The array used in the set-up is an 56 microphone array. It is planar and has a layout that consists of 5 circles with 16 or 8 microphones each. The aperture of the array, defined by the largest distance between two microphones from the array, is 1.30 m. The microphone signals were sampled at a rate of 51.2 kHz. An FFT with prior von Hann weighting was applied for every channel to 1000 consecutive, 50% overlapping blocks of 4096 samples each. All 56^2 cross spectra were calculated and averaged over the 1000 blocks to produce the cross spectral matrix. Two different grids were used for the source mapping (2). The first grid is a two-dimensional

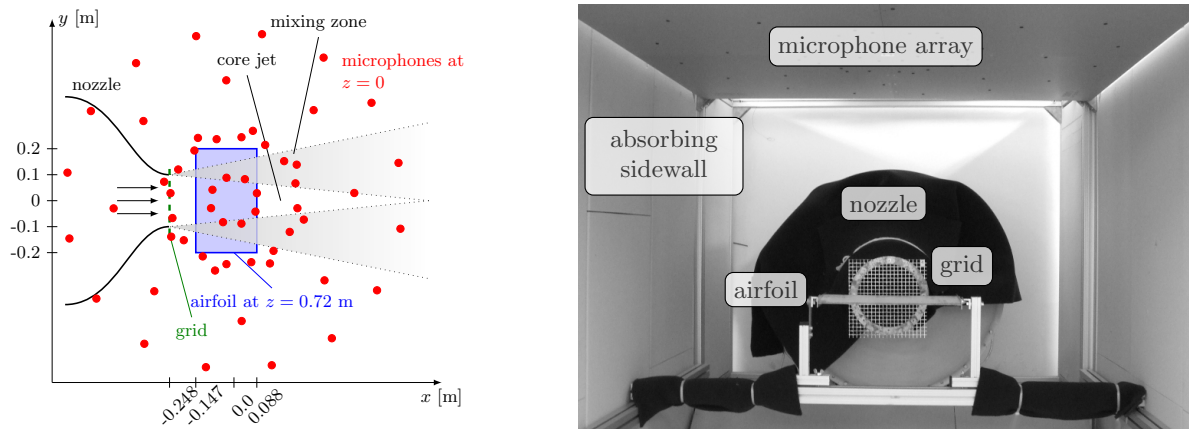

(a) schematic (view from above) (b) photographic view from downstream

Figure 1: Measurement set-up

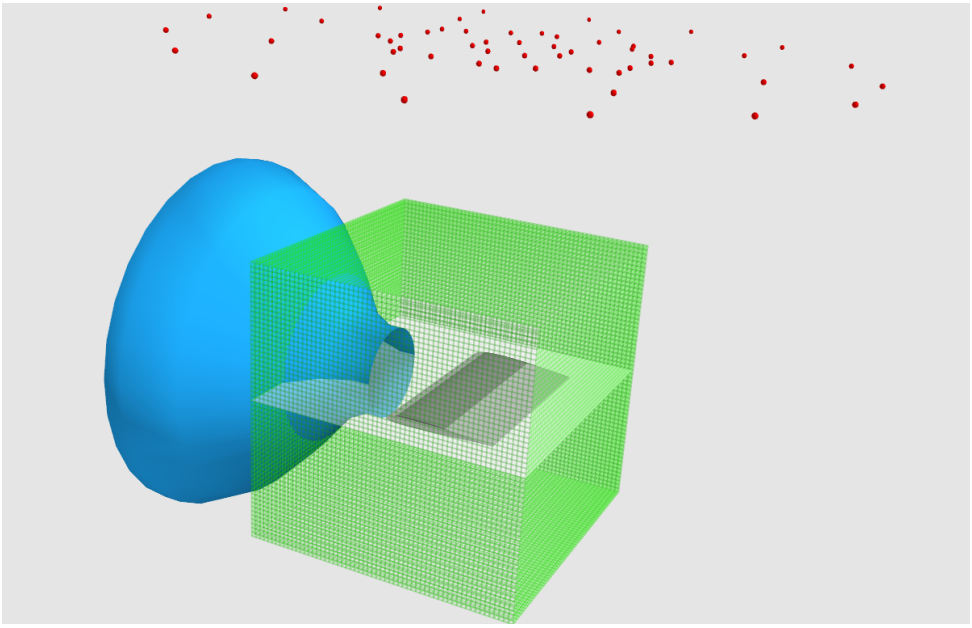

Figure 2: Three-dimensional schematic of the set-up with nozzle (blue), array (red), aerofoil (grey), two-dimensional grid plane (white), three-dimensional grid (green), turbulence grid in the nozzle is not shown

planar grid of 0.6 m ×0.6 m and a uniform grid spacing of 1 cm that has 3721 grid points. The second, three-dimensional grid has an extra extent of 0.6 m in the third dimension and the same grid spacing. The overall number of grid points is 226,981.

Fig. 3 illustrates the need for the application of a deconvolution technique in this case. The two-dimensional mapping using conventional beamforming as in equation 2 shows that the turbulence grid in the nozzle is a major source. However, no distinct sources at leading or trailing edge can be identified from the mapping. Instead, a number of 'sources' appear at

random locations, even outside the flow. The two-dimensional mapping using CLEAN-SC deconvolution reveals the sources at leading and trailing edge and the sources outside the flow disappear. When it comes to three-dimensional mapping, conventional beamforming fails to produce a meaningful result. While in the nozzle region a major source appears to exist, many more sources appear all over the mapping region. The CLEAN-SC result, however, shows very clearly the extent of the source at the turbulence grid at the nozzle as well as the sources at both leading and trailing edge. It can be concluded that while the two-dimensional result is improved by deconvolution, deconvolution is absolutely necessary in the case three-dimensional mapping, because only then a meaningful result is produced.

To further explore the differences of two- and three-dimensional mapping, Fig. 4 shows sound maps for two third-octave bands. At 6.3 kHz the sound generation at the grid itself dominates and the sound generation at both the leading and the trailing edge is barely visible. At 2 kHz, the sound generation at the airfoil dominates. The maps show some more details as the sound generated by the the interaction of the shear layer of the wind tunnel jet and the airfoil, but also sound generated at the edge of nozzle. Figs. 4 (a) and (b) show the usual two-dimensional mapping. The sources at the leading and the trailing edge can be expected to lay within or near the mapping plane. The sources at the nozzle are mostly out of the plane. Consequently, they are mapped to locations in the plane. The nature of this effect can be understood by comparing to Figs. 4 (c) and (d) that show a slice from the three-dimensional mapping. The location of this slice coincides with that of the two-dimensional mapping plane and shows more clearly the real contribution from that plane. At least a part of the leading edge and the turbulence grid (in the case of 6.3 kHz) noise appears. The trailing edge is situated somewhat (about 1.5 cm) below the plane (see Fig. 2). Consequently, the trailing edge noise does not appear in the this slice. Figs. 4 (e) and (f) show a two-dimensional projection of the three-dimensional mapping, where the contributions from all planes parallel to the two-dimensional mapping plane are accumulated. This result is similar to the two-dimensional mapping, but shows also some quantitative differences.

Quantitative results from acoustic source mappings can be produced by integration over sectors of the map. If the map is produced by conventional beamforming, the beamformer filter properties must be considered in this process (see e.g. [10]). In contrast to this, a deconvolved map can be integrated as is. Consequently, this integration technique can be adopted for three-dimensional deconvolved maps. The only difference is that the integration must be limited to a volume instead of a planar sector. For the example of leading edge noise, Fig. 5(a) shows this volume. In Fig. 5(b), the results from the integration of the two-dimensional and the three-dimensional mapping are compared. It can be seen that there are only negligible differences in the higher frequency range that become somewhat larger in the low frequency range. It can be concluded that the quantitative error in the two-dimensional mapping is somewhat larger at these frequencies.

Finally, the computational cost for the three-dimensional mapping should be considered. While it would be possible to compare the number of necessary floating point operations, it is obvious that the time needed for the computation depends also on the amount of data that must be transferred during calculation. Moreover, the computing hardware as well as the software implementation and optimization matters. To illustrate the differences, some data is given for the authors implementation of conventional beamforming and CLEAN-SC (using PYTHON/Numpy [1] with optimized C++ extensions) running under Linux on an Core

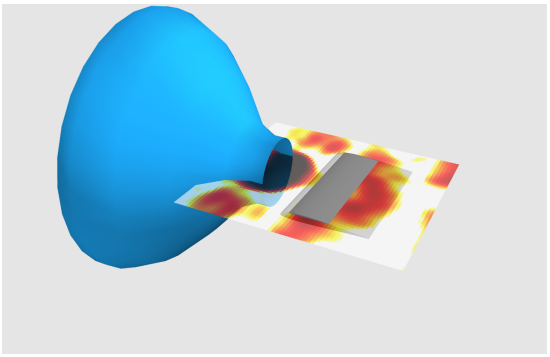

(a) two-dimensional mapping, conventional beamforming

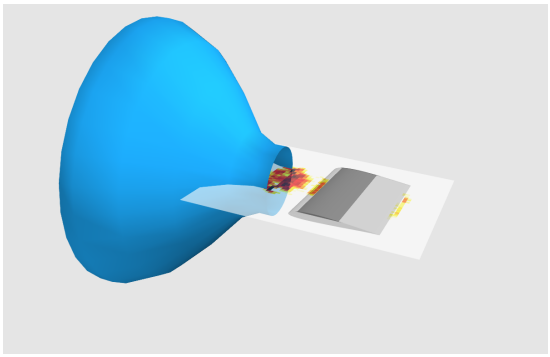

(b) two-dimensional mapping, CLEAN-SC

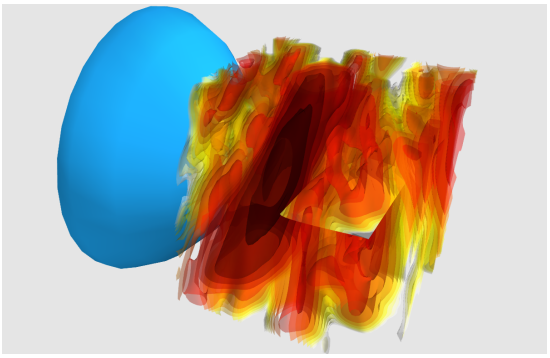

(c) three-dimensional mapping, conventional beamforming

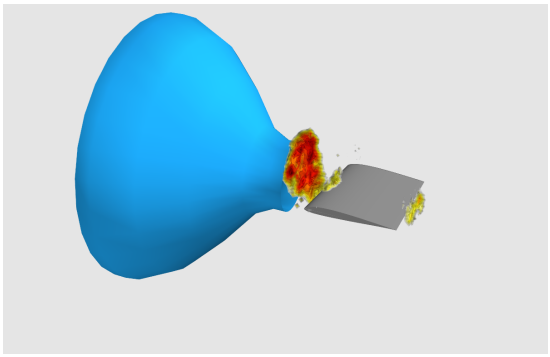

(d) three-dimensional mapping, CLEAN-SC

Figure 3: Sound maps at 6.3 kHz from two- and three-dimensional mapping, 35 dB dynamic range

Table 1: Computing times per frequency

	2D-mapping, 3721 grid points		3D-mapping, 226,981 grid points	
	conventional beamforming	CLEAN-SC	conventional beamforming	CLEAN-SC
single core	26 ms	1.0 s	6.2 s	75 s
parallel processing (8 cores)	9 ms	180 ms	0.9 s	13 s

i7 multi-core PC. Table 1 shows mean times needed for the computation of the mapping per frequency. The data shows clearly that three-dimensional mapping requires considerably more effort, but the time is still within acceptable limits for practical application, especially if the multi-core capabilities of the hardware are used. The data shows also that any deconvolution technique that needs considerably more computational effort than CLEAN-SC will not be feasible for practical application in this case.

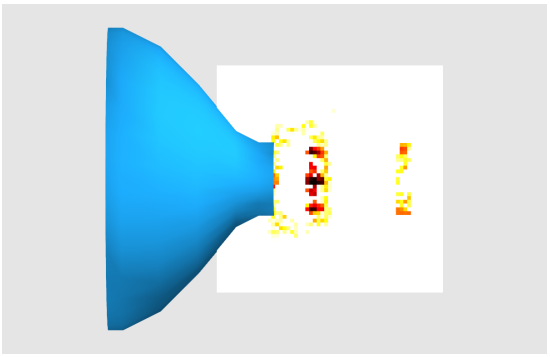

(a) 2 kHz, two-dimensional mapping

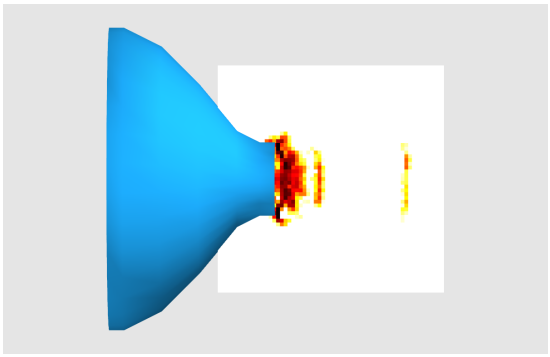

(b) 6.3 kHz, two-dimensional mapping

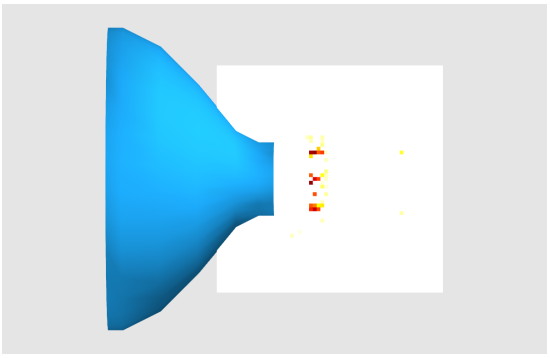

(c) 2 kHz, slice at z=0.71 m from three-dimensional mapping

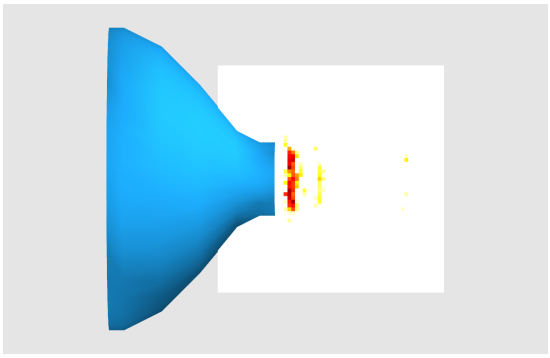

(d) 6.3 kHz, slice at z=0.71 m from three- dimensional mapping

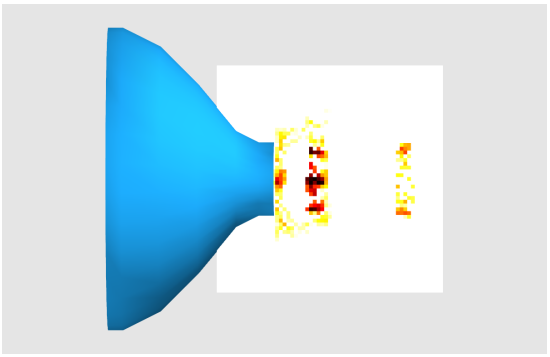

(e) 2 kHz, two-dimensional accumulated projection of three-dimensional mapping

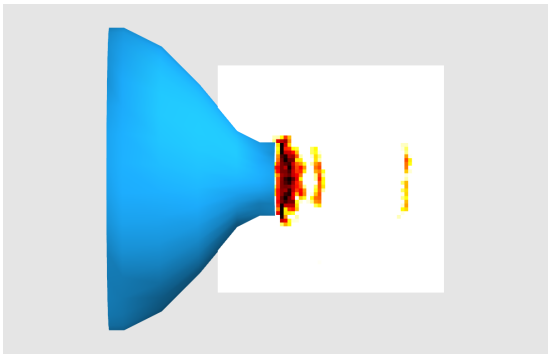

(f) 6.3 kHz, two-dimensional accumulated projection of three-dimensional mapping

Figure 4: Sound maps from two- and three-dimensional CLEAN-SC mapping, 35 dB dynamic range, same scale for all 2 kHz results, and same scale for 6.3 kHz results

4 CONCLUSIONS

Three-dimensional acoustic source mapping for the purpose of the study of acoustic sources is straightforward to implement. However, the result will only be meaningful if a deconvolution technique is applied. Then, the mapping delivers additional information about the location

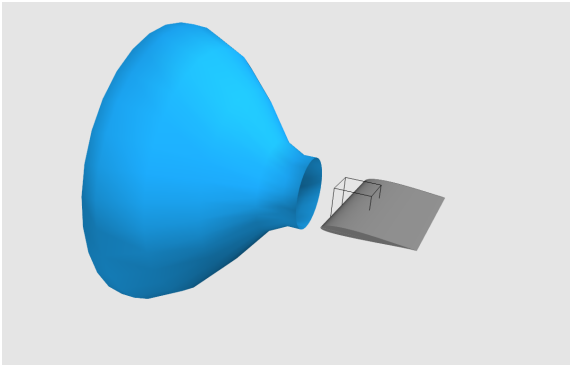

(a) integration volume

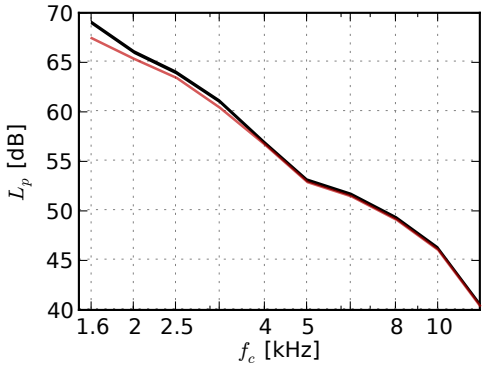

(b) spectra from two- (black) and three-dimensional (red) mapping

Figure 5: Third octave band spectrum of the sound pressure level at the array centre for leading edge noise

of sources and yields quantitatively correct results. Spectra of the contribution from partial sources can be estimated by a three-dimensional integration of the map. The computational cost is considerable higher than for classical two-dimensional mapping, but provided an efficient deconvolution method, it is still acceptable.

References

[1] URL `http://www.scipy.org`.

[2] H. Brick, T. Kohrs, E. Sarradj, and T. Geyer. "Noise from high-speed trains: Experimental determination of the noise radiation of the pantograph." In *Forum Acusticum 2011, Aalborg*. 2011.

[3] T. F. Brooks and W. M. Humphreys, Jr. "A Deconvolution Approach for the Mapping of Acoustic Sources (DAMAS) Determined from Phased Microphone Arrays." AIAA-2004-2954, 2004. 10th AIAA/CEAS Aeroacoustics Conference, Manchester, Great Britain, May 10-12, 2004.

[4] T. F. Brooks and W. M. Humphreys, Jr. "Three-Dimensional Applications of DAMAS Methodology for Aeroacoustic Noise Source Definition." AIAA-2005-2960, 2005. 11th AIAA/CEAS Aeroacoustics Conference, Monterey, California, May 23-25, 2005.

[5] R. P. Dougherty. "Jet noise beamforming with several techniques." BeBeC-2010-17, 2010. URL `http://bebec.eu/Downloads/BeBeC2010/Papers/BeBeC-2010-17.pdf`, proceedings on CD of the 3rd Berlin Beamforming Conference, 24-25 February, 2010.

[6] T. Geyer, E. Sarradj, and J. Giesler. "Application of a beamforming technique to the measurement of airfoil leading edge noise." *Advances in Acoustics and Vibration*, 2012. URL `http://www.hindawi.com/journals/aav/2012/`.

[7] K. Oakley. "NoiseCam – Using 3D Beamforming to better localise noise sources on Hovercraft." BeBeC-2010-22, 2010. URL `http://bebec.eu/Downloads/BeBeC2010/Papers/BeBeC-2010-22.pdf`, proceedings on CD of the 3rd Berlin Beamforming Conference, 24-25 February, 2010.

[8] E. Sarradj. "A fast signal subspace approach for the determination of absolute levels from phased microphone array measurements." *J. Sound Vib.*, 329(9), 1553–1569, 2010. doi: 10.1016/j.jsv.2009.11.009.

[9] P. Sijtsma. "CLEAN Based on Spatial Source Coherence." AIAA-2007-3436, 2007. 13th AIAA/CEAS Aeroacoustics Conference, Rome, Italy, May 21-23, 2007.

[10] P. Sijtsma and R. Stoker. "Determination of Absolute Contributions of Aircraft Noise Components Using Fly-over Array Measurements." AIAA-2004-2958, 2004. 10th AIAA/CEAS Aeroacoustics Conference, Manchester, United Kingdom, 10-12 May 2004.